Quaternary International xxx (2017) 1–12

Contents lists available at ScienceDirect

Quaternary International

journal homepage: www.elsevier.com/locate/quaint

Geochronology and paleoenvironment of the Taoshan site, northeastern China, and archaeological implications

Guan-Nan Zou [a, b], Gideon Shelach [c], Xiao-Qiang Li [d], Chao Zhao [d, e], Xue Rui [a, f], Li-Ping Zhou [a], Jia-Fu Zhang [a, *]

[a] MOE Laboratory for Earth Surface Processes, Department of Geography, College of Urban and Environmental Sciences, Peking University, Beijing, 100871, China
[b] Yuanpei College, Peking University, Beijing, 100871, China
[c] Department of Asian Studies, Hebrew University, Jerusalem, 91905, Israel
[d] Key Laboratory of Vertebrate Evolution and Human Origins of CAS, Institute of Vertebrate Paleontology and Paleoanthropology, CAS, Beijing, 100044, China
[e] Institute of Geographic Sciences and Natural Resources Research, CAS, Beijing, 100101, China
[f] Centre for Archaeological Science, School of Earth and Environmental Sciences, University of Wollongong, Wollongong, NSW, 2522, Australia

ARTICLE INFO

Article history:
Received 29 February 2016
Received in revised form
16 June 2017
Accepted 30 June 2017
Available online xxx

Keywords:
Luminescence and radiocarbon dating
Paleoenvironmental reconstruction
Climate change
Stone artifacts and pottery
Neolithization
Northeastern China

ABSTRACT

The Taoshan archaeological site located in northeastern China was found in 2011, and an area of 36 m^2 was excavated in 2013 and 2014. 2908 stone artifacts, 71 pottery fragments and five ornaments were excavated from three cultural layers. Similar sites with both stone artifact and pottery at least in Heilongjiang Province of China have not been reported. The dating results showed that the optically stimulated luminescence technique is of great utility for such archaeological deposits, and the three cultural layers were dated to 16.5–13.4 ka, 13.4–8.7 ka and 8.7–5.6 ka, respectively. The climate proxies (magnetic susceptibility, total organic content and pollen) indicate that the local climate was cold and dry for the period of 16.5–13.4 ka, warm and wet for the period of 13.4–8.7 ka and warm and dry for the period of 8.7–5.6 ka, respectively. The types and amount of archaeological findings from each layer (period) reflect the human response to the past climate change, implying that the human-related processes identified at Taoshan are associated with climatic and environmental changes. The investigations of the site are very important for developing a better understanding of the colonization of this region by humans, the transmission of technologies and the processes of economic and social change the local societies underwent. The presence of microblades and pottery is the most significant for our reconstructing of the archaeology of the northernmost parts of Northeast China.

1. Introduction

The Taoshan archaeological site (46°54.765′N, 128°12.643′E) is located at the Taoshan town, Tieli County of Heilongjiang Province, northeastern China, and is about 180 km to the northeast of Harbin, the capital of Heilongjiang Province (Fig. 1a). An area of 36 m^2 (Fig. S1) was excavated during the two excavation seasons in 2013 and 2014, and 2908 stone artifacts and 71 pottery sherds and five ornaments were recovered. The stone artifacts include cores, scrapers, denticulates, notchs, borers, arrowheads, microcores, microblades and blades (Fig. 2). No animal fossils have been found. Similar archaeological sites with both pottery and stone artifact in Heilongjiang Province have not been reported.

Although not yet fully published, Taoshan is already recognized as a significant site that contribute to our understanding of the archaeology of the northernmost parts of Northeast China (Chang et al., 2016; Yue et al., 2017; Yang et al., 2017). From archaeological perspective the presence of microblades and pottery is the most significant. Similar technologies and types of artifacts are known from contemporaneous and even earlier sites in other parts of North China as well as from the Amur region to the north. Early microblades are found, for example, at the Longwangchan site in Hukou, Shaanxi (Zhang et al., 2011; Zhongguo Shehui Kexueyuan Kaogu Yanjiusuo and Shaanxi Sheng Kaogu Yanjiusuo, 2007) dated to ca. 23.0 ka and at sites ascribed to the *Xiachuan* culture of the southern Shanxi province and dated to ca. 18.0 ka (Chen, 2007;

* Corresponding author.
E-mail address: jfzhang@pku.edu.cn (J.-F. Zhang).

http://dx.doi.org/10.1016/j.quaint.2017.06.073
1040-6182/

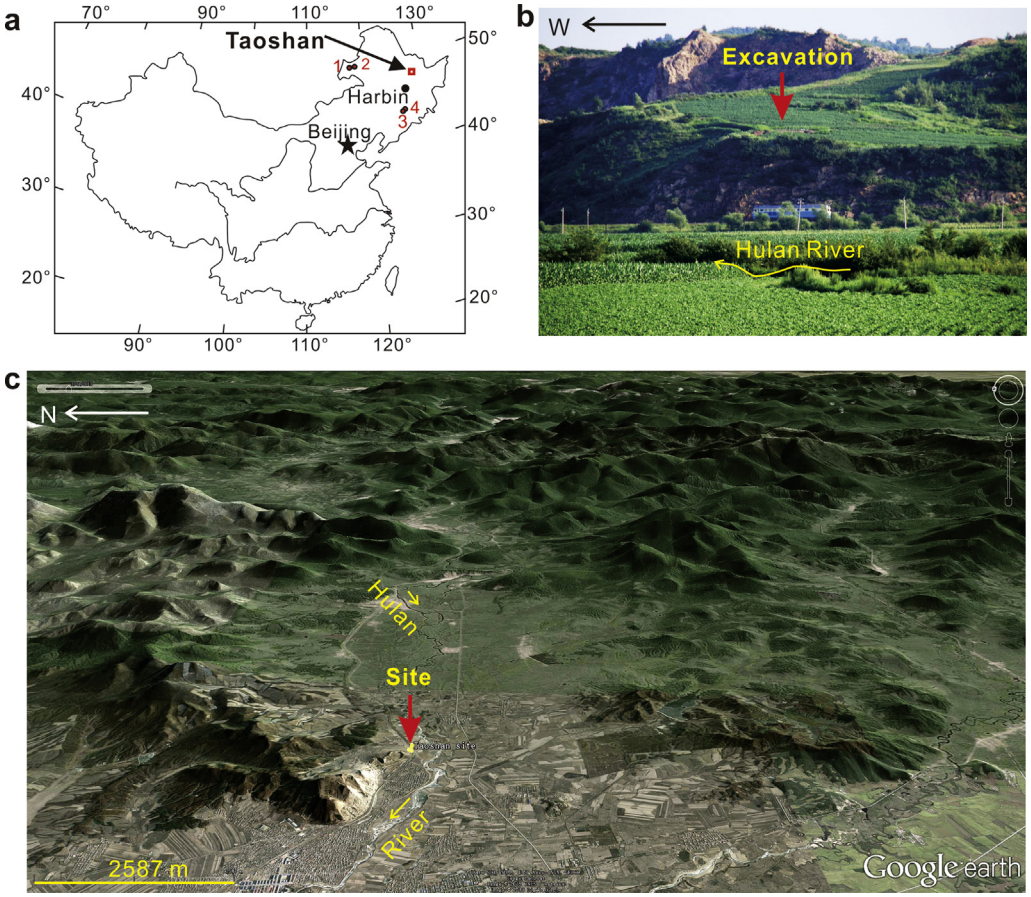

Fig. 1. (a) Map showing the locations of the Taoshan site, and Hulun Lake (1), Hulun Buir Desert (2), Hani peat bog (3) and Lake Sihailongwean (4) mentioned in text and Fig. 7; (b) photograph (looking north) showing the excavation site on a slope and the Hulan River on the basin; (c) Google Earth satellite image showing the landscape features of the studied region, the Hulan River flows through the basin.

Wang et al., 1978). A good example for an early Holocene site of macroblades are found is Donghulin in the Beijing area (Beijing Daxue, 2006) but microblades are typical to most sites of this period in North China (Bettinger et al., 2007; Chen, 2007; Shelach, 2015). Well preserved examples for early ceramics in North China were found at the site of Nanzhuangtou in Hebei province, dated to ca. 10.0–8.0 ka (Baoding, 1991; Guo and Li, 2002; Hebei Sheng Wenwu Yanjiusuo et al., 2010); and see references to other sites in North China (Shelach, 2015) and the Amur (Kuzmin, 2006). However, such artifacts were rarely if ever found in Heilongjiang. Although Heilongjiang was not one of the centers where agriculture developed independently and, in fact, it never evolved into a primarily agricultural center, the processes whereby populations and technologies filtered into new areas and the interaction between different kinds of populations are significant dynamics in human history. Thus, the study of Taoshan can contribute much to our understanding not only of the history of this particular region but of a more general anthropological issues.

The exact chronology of the Taoshan site and the analysis of the artifacts found in it, as well as the ecological context of the cultural and economic change they represent, are important for developing a better understanding of the colonization of this region by humans, the transmission of technologies and the processes of economic and social change the local societies underwent. This site can also help us to better understand cultural response to climate change in northeastern China (Borrero et al., 1998; Berglund, 2003; Yasuda et al., 2004; Guo et al., 2014; Naudinot and Kelly, 2017). The local paleoclimate is relatively unknown and few paleooecological studies have been conducted in this area. Even for the northeastern China, only paleoclimatic records from a few localities such as Hani (Seki et al., 2009; Zhou et al., 2010), Hulun Buir Desert (Li et al., 2002; Li and Sun, 2006), Hulun Lake (Wen et al., 2010) and Lake Sihailongwan (Stebich et al., 2015) (Fig. 1a) have been published. The lack of local paleoenvironmental data hinders our understanding of the relationship between human occupation and the natural habitat. In this study, the chronology of the site was determined using radiocarbon and optically stimulated luminescence (OSL) dating methods, and the paleoclimate was reconstructed from multiple climate proxies. By correlating these data with the findings at different archaeological strata of the Taoshan site, we reconstruct the sequence of human occupation at the sites. Such an analysis is relevant to a more general discussion about the human colonialization of this region. Findings such as pottery are also relevant to address the filtering of new technologies into the region and the evaluation of the process of 'Neolithization'.

2. Geomorphological setting, stratigraphy and archaeological contexts

2.1. Geomorphological setting

The study area is located at the transition zone from a mountainous region to an extensive plain region (Songnen Plain) to the west. The mountains are primarily composed of andesitic and

Please cite this article in press as: Zou, G.-N., et al., Geochronology and paleoenvironment of the Taoshan site, northeastern China, and archaeological implications, Quaternary International (2017), http://dx.doi.org/10.1016/j.quaint.2017.06.073

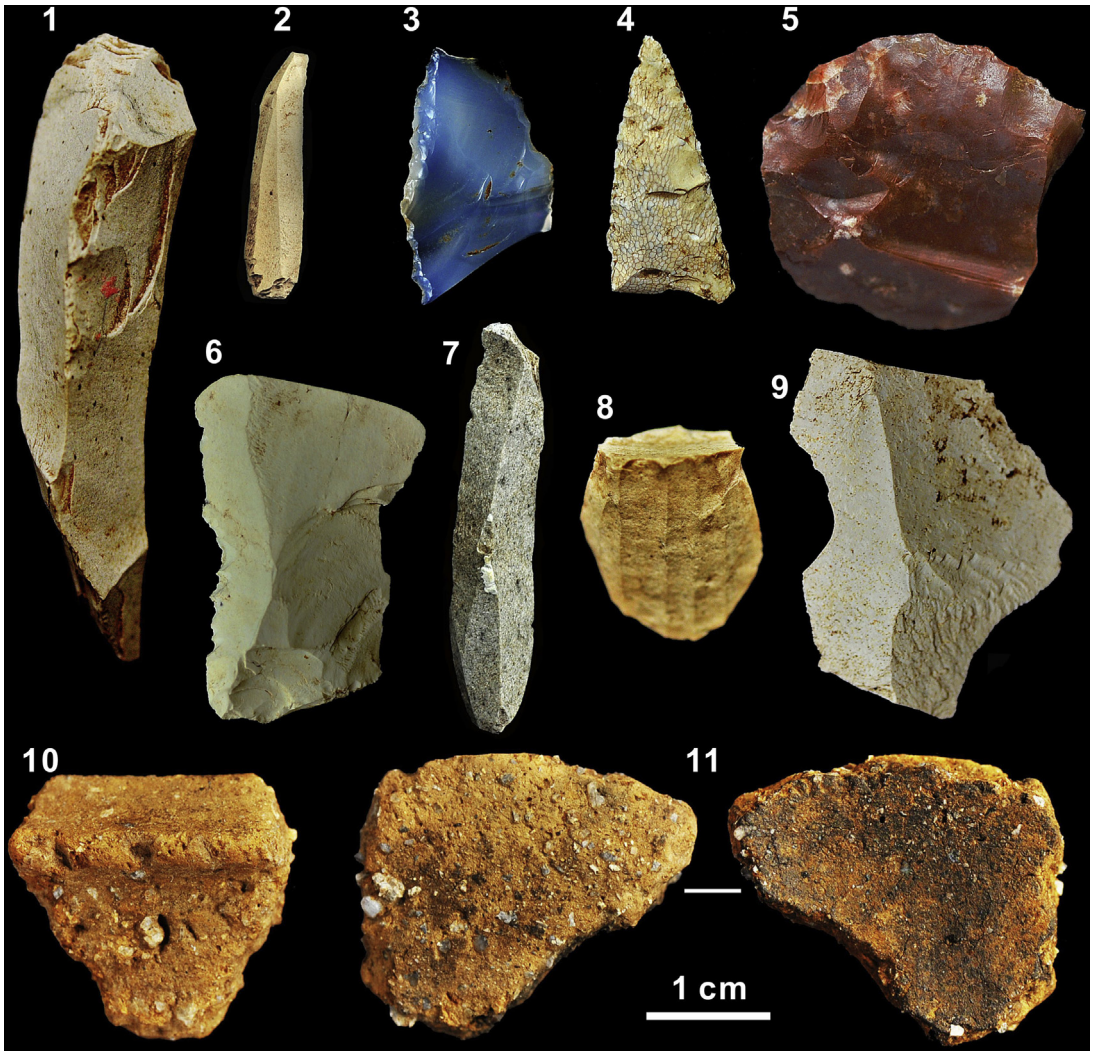

Fig. 2. Photographs showing the stone artifacts and pottery sherds excavated from the Taoshan site. 1: Crested blade, 13TS(3)C15:873; 2: Microblade, 14TS(3)B17:1384; 3: Scraper, 13TS(2)B19:243; 4: Arrowhead, 13TS(2)A20:463; 5: Scraper, 13TS(2)A20:553; 6: Denticulate, 13TS(3) F19:136; 7: Microblade, 14TS(3)B16:803; 8: Microcore, 13TS(3)C15:871; 9: Notch, 13TS(3)13TS(3)F20:301; 10: Pottery sherd, 13TS(2)C19:67; 11: Pottery sherd, 13TS(2)A18:354. The values in brackets refer to the layer from which the artifacts and pottery sherds come.

rhyolithic pyroclastic rocks and lava and sandy conglomerate of Jurassic age. The Taoshan site is situated on a mountain slope facing a ~45 km^2 intermontane basin (Fig. 1b and c). The basin is surrounded by mountains on three sides. The elevation of the highest mountain is up to about 1000 m above sea level (asl) in the west, and 800 m asl in the south. The elevation of the basin varies from about 260 m (asl) in the east to about 220 m asl in the west. The floor of the basin slopes gently towards the north part, and is occupied by farmlands. To the south of the basin, there is Songnen Plain from which many upper Paleolithic sites have been found (Kato, 2016). The basin deposits consist mainly of alluvial sediments. The Hulan River flows through the basin from east to west, and sinuous meanders developed on the river. The river is a tributary of the Songhua River in Heilongjiang, and originates in the northeastern mountains. From its source to the town of Taoshan, the river length and the drainage area is about 80 km and about 1500 km^2, respectively, and the stream gradient is about 0.2%.

The site area is relatively flat, and covered by shrubs and crops. Its bedrock is granite, which is widely used for building materials by local people, and its peak is about 500 m asl. The site is at about 241 m asl and 21 m higher than the modern Hulan River, and bounded by a 13-m high bedrock cliff to the south. The climate of the studied area is strongly influenced by the Asian summer monsoon with an average annual modern precipitation of about 630 mm mainly occurring during the summer season. According to the local meteorological station, the average annual modern temperature is about 1.4 °C (−23.1 °C for January and 21.4 °C for July).

2.2. Stratigraphy and archaeological contexts

The Taoshan site discovered in 2011 was excavated in 2013 and 2014 by a joint archaeological team of Institution of Vertebrate Paleontology and Paleoanthropology, Chinese Academy of Sciences and Cultural Relics and Archaeology of Heilongjiang Province led by archaeologist Yamei Hou. The excavation proceeded by cultural levels, the area of 36 m^2 was divided into thirty-six 1 × 1 m archaeological excavation units (Fig. S1) (Chang et al., 2016; Yue et al., 2017). The excavations revealed that the deposits are dominantly composed of clayey silts. They have a massive structure (unstratified), and are loose and porous and with grey brown to

Please cite this article in press as: Zou, G.-N., et al., Geochronology and paleoenvironment of the Taoshan site, northeastern China, and archaeological implications, Quaternary International (2017), http://dx.doi.org/10.1016/j.quaint.2017.06.073

brown yellow color. Accordingly, we interpret these sediments as aeolian in origin. The geomorphological setting implies that some grains might move downslope in occasional heavy rain storms. For the whole excavation area, the thickness of the entire sediment sequence varies from about 70 to 90 cm, and its properties are relatively simple and uniform. A typical section is shown in Fig. 3a and Fig. S2, and is divided into four stratigraphic layers in the field. The transitions between layers are gradual. Stone artifacts were mainly found in the cultural layers (Layers 2, 3 and 4, corresponding to archaeological phases (Phases 2, 3 and 4)), and the raw materials are mainly made up of tuff, agate, dolomite, basalt and chert, and pottery sherds are from Layers 2 and 3. No animal fossils were retrieved from the site (Chang et al., 2016; Yue et al., 2017).

The bottom layer (Layer 4) is a loess layer, and directly overlies granite bedrock. This 20–30-cm-thick layer comprises of brown yellow sandy clayey silt with a few weathered rock fragments of variable sizes. We deduce that the fragments come from the granite bedrock of the study area. This layer contains about 275 stone artifacts including flakes, blades, scrapers and chunks.

Layer 3 is composed of 10–20-cm-thick organic-rich sandy clayey silt, with occasional weathered rock fragments with sizes of 3–5 cm in diameter. This layer is clearly distinguished from overlying (Layer 2) and underlying (Layer 4) layers by its dark grayish brown color, and was thus interpreted as buried soil. A total of 2006 stone artifacts and 24 pottery sherds were recovered from this layer. The artifacts include flakes, microblades, microcores, tools and debitage. The tools include forms of notches, denticulates and scrapers.

Layer 2 consists of brown yellow clayey silt with massive structure. This loess layer varies 4–25 cm in thickness, from which 627 stone artifacts, 47 pottery sherds and five ornaments have been unearthed. The artifacts include flakes, microblades, microcores, tools and debitage. The tools include forms of scrapers, denticulate, notches, borers, burins, awls, arrowheads, endscrapers and choppers.

The top layer (Layer 1) is composed of 10 to 20-cm-thick soils developed on the mountain slope. The loose and dark brown soils are being cultivated. Pieces of maize straw found indicates that this layer has been reworked by agricultural activities. A few stone artifacts were recovered, and considered from the underlying cultural layer (Layer 2) due to human agricultural activities.

All the stone artifacts are not abraded and relatively complete, and have no preferential orientation (i.e., azimuth and inclination). Several refitted groups of artifacts were also found. All the evidence indicates that they were buried in-situ. From the refitting analyses and the existence of debitage we deduce that manufacturing and retouching activities were conducted at the site (Chang et al., 2016; Yue et al., 2017).

3. Samples and methods

3.1. Samples

A total of eight sedimentary samples for OSL dating were collected from the north section of Square F19 (Fig. S1 and Fig. 3a). The OSL samples were taken by inserting clean metal canisters into the excavated section. After taking the canisters out, their ends were capped and then sealed with aluminum foil and tape. Five charcoal samples for radiocarbon dating were collected from Layers 2–4. It is noted that the charcoal fragments are from other squares of the site (Fig. S1). The section of Square F19 was also sampled for paleoenvironmental proxy analyses, including particle-size analysis, magnetic susceptibility (MS) measurement and total organic carbon (TOC) determination. A total of 72 such samples were taken at an interval of 1 cm. Additionally, two sediment samples from each cultural layers and one sample from the top soil were collected for pollen analysis.

3.2. Particle size analysis and magnetic susceptibility measurement

The grain-size distributions of the samples were analyzed using a Malvern Mastersizer 2000 laser grain size analyzer, which determines vol% in 100 grain-size classes ranging from 0.02 to 2000 μm in diameter, corresponding to an interval of 0.166 ϕ (ϕ=-$\log_2(D)$, D=the grain diameter in mm). The Mie-theory was used for calculating (Malvern software version 5. 12C) the grain-size distributions. Before measurement, the samples of <2 mm in diameter were first chemically treated with 30% hydrogen peroxide at room temperature to digest organic material, and 10% dilute hydrochloric acid to remove carbonates. The samples were then dispersed in a solution of $(NaPO_3)_6$ and additionally kept in ultrasonic bath prior to measurement. After each step, the sample solution was boiled to further remove remaining organic matter, carbonates, or to fully dissolve the dispersant ($(NaPO_3)_6$. After 3-min sonication in deionized water, each sample solution was analyzed three times. The results of one measurement was reported.

For magnetic susceptibility (MS) measurements, the samples were air-dried in laboratory, and then weighed and packed into small plastic boxes. Mass specific, low frequency MS was determined using a Bartington MS2 meter with a MS2B sensor at 0.1 SI sensitivity, and the MS values are expressed in SI units ($10^{-8}m^3kg^{-1}$).

3.3. Total organic carbon determination

The samples for total organic carbon (TOC) measurements were first air-dried, and then ~50 mg of each sample was weighed and treated by 5% H_3PO_4 to remove carbonates (inorganic carbon, IC). Following that, the samples were burned in a muffle furnace at 900 °C for 10 min to convert organic carbon to carbon dioxide measured by a Shimadzu TOC-V_{CPN} analyzer.

3.4. Pollen and charcoal analysis

Samples were prepared for pollen analysis and charcoal counting using conventional methods including an acid-alkali treatment (hydrochloric acid, potassium hydroxide and acetolysis) and heavy liquid flotation (Faegri and Iversen, 1989; Li and Du, 1999). *Lycopodium* tablets were added to count the pollen and charcoal concentration (Peck, 1974). 150–200 pollen and spore grains for samples 14TS A17(2) and 14TS C17(4) and 250–600 grains for other samples were counted. Pollen percentage and concentration were calculated only based on the total terrestrial pollen sum (100%). Charcoal measurements are reported as total charcoal area concentration per volume of sediment (mm^2 cm^{-3}) (Clark, 1988). The pollen percentage diagram was drawn using the computer program TILIA (Grimm, 1990).

3.5. Dating

3.5.1. Luminescence dating

Fine-grained (4–11 μm) quartz for OSL measurement was chemically extracted from the studied samples using the procedure in the Luminescence Dating Laboratory at the Peking University (Zhang and Zhou, 2007). The procedure involves the removal of carbonates and organic materials using HCl and H_2O_2, the extraction of polymineral fine grains based on the Stokes' Law, and the purification with silica saturated fluorosilicic acid (H_2SiF_6). The purity of the quartz extracts obtained was checked using IR stimulation. No detectable infrared stimulated luminescence signals

Please cite this article in press as: Zou, G.-N., et al., Geochronology and paleoenvironment of the Taoshan site, northeastern China, and archaeological implications, Quaternary International (2017), http://dx.doi.org/10.1016/j.quaint.2017.06.073

were observed, suggesting that feldspar contaminants were completely removed. The aliquots for OSL measurement were made by settling the fine grains in acetone onto 0.97 cm diameter aluminum discs.

Equivalent dose (D_e) was determined using the improved single-aliquot regenerative-dose (SAR) protocol (Murray and Wintle, 2000; Wintle and Murray, 2006). A total of five beta irradiations were performed, including a zero-dose used for monitoring recuperation effects and a repeat of the first regeneration dose used for checking the reproducibility of the sensitivity correction (i.e. recycling ratio). The preheat temperature was determined by preheat plateau and dose recovery tests. OSL signals were measured for 40 s at 125 °C, and a cut-heat of 160 °C was applied. The net initial OSL signals were derived from the decay curve, taking the first 0.64 s integral of the initial OSL signal, minus a background estimated from the last 3.2 s integral of a 40 s stimulation. The value of D_e was estimated by interpolating the sensitivity-corrected natural OSL onto the dose-response curve. Only 5–7 aliquots for each sample were measured because the measured aliquot's D_e values obtained for a sample are almost identical. Luminescence measurements, beta irradiation and preheat treatments were carried out in an automated Risø TL/OSL-15 reader equipped with a $^{90}Sr/^{90}Y$ beta source (Bøtter-Jensen et al., 1999). Blue light (470 ± 30 nm) LED stimulation was used for OSL measurements. Luminescence was detected by an EMI 9235QA photomultiplier tube with a 7.5 mm Hoya U-340 filters (290–370 nm) placed in front of it.

Neutron-activation-analysis measured U, Th and K contents used for dose rate calculation were analyzed by, and water contents (mass of moisture/dry mass) were determined by weighing the samples before and after drying in an oven. It is noted that the water contents were estimated at ~15% for the three samples from Layer 4, and ~17% for the five samples from Layers 2 and 3. Based on the sedimentary properties mentioned above and the water content of overlying samples, we determined that the water content of 15% for the three samples from Layer 4 was underestimated. We thus used a water content of 17% in the dose rate calculations. The effective dose rate and OSL ages were calculated using the computer program "DRcalculator" published by Tsakalos et al. (2015), in which all parameters involved in the calculation are presented.

3.5.2. Radiocarbon dating

The charcoal samples were pretreated in the School of Archaeology and Museology at Peking University (Zhang et al., 2011; Wu et al., 2012). In the laboratory, hard and compact pieces of charcoal fragments were selected for further analyses by hand-picking under a stereo microscope, assuring that the dated samples were in a good state of preservation and appeared not to have been altered. All visible contaminants such as plant roots were removed. The selected samples were cleaned in an ultrasonic bath with distilled water and then chemically pretreated with the standard AAA (Acid-Alkali-Acid) procedure consisting of treatments with 0.5 N HCl, 1 N NaOH and dilute HCl. All pretreated samples were weighed into quartz tubes together with CuO and Ag. The tubes were evacuated, flame-sealed and combusted at 850 °C. The CO_2 generated was purified and converted to graphite by reduction with H_2 gas using Fe powder as a catalyst. The graphite obtained was then pressed into target holders for analysis with the compact AMS facility at the Institute of Heavy Ion Physics of Peking University (Liu et al., 2007). The radiocarbon ages obtained were converted into calendar years using the online OxCal V4.2 software (Bronk Ramsey, 2009) and the IntCal13 calibration curve (Reimer et al., 2013). Calibrated radiocarbon ages (cal. ka BP or cal. yr BP) are used for comparison with OSL ages.

4. Results

4.1. Grain-size distribution and magnetic susceptibility

The grain-size distributions obtained for the studied section are shown in Fig. 4. Based on their distribution patterns, the samples can be categorized into two groups: Group 1 consists of the upper samples from the depths of 0–36 cm, and Group 2 is composed of the lower samples from the depths of 36–73 cm. All the samples are dominated by silt, with minor clay and sand. Relatively, the Group 2 samples contain coarser and more sand. This is also demonstrated by their mean grain sizes shown in Fig. 3c. The average mean grain sizes of the Groups 1 and 2 samples are about 15 and 27 μm, respectively. It can also be seen that Layers 4 and 3 are mainly composed of the Group 2 samples, and Layers 1 and 2 comprise the Group 1 samples. The low frequency MS average values for Layers 4–1 are 9.2, 12.5, 13.5 and 15.3 × $10^{-8}m^3kg^{-1}$, respectively. The MS variations with depth shown in Fig. 3d indicate that the MS values generally increases with decreasing depth, and are relatively constant within each layer for Layers 4, 2 and 1.

4.2. TOC

The TOC contents shown in Fig. 3e indicate that the TOC contents are higher in soils (Layers 3 and 1), and lower in loess (Layers 4 and 2), as suggested by their colors. The average TOC values for Layers 4 to 1 are 0.5%, 0.8%, 0.6% and 2.6%, respectively. The largest TOC content in the topsoil may be caused by the presence of highly decomposable organic matter, such as pieces of modern maize straw.

4.3. Pollen and charcoal

A total of 42 pollen taxa were identified. The percentage diagrams and total pollen and charcoal concentrations as a function of depth are presented in Fig. 5. Based on the characteristics of pollen assemblages, charcoal concentration and inferred vegetation, the section is divided into four pollen zones that coincide with the archaeological and stratigraphic layers. Layer 4 is characterized by low vegetation coverage and relatively high concentration of charcoal. The vegetation cover was dominated by steppe with Chenopodiaceae and *Artemisia*; sparse and mixed coniferous and broadleaf forest grew on the uplands of the area during the time when Layer 4 was being deposited. The buried soil layer (Layer 3) has a relatively high pollen concentration, and its pollen assemblage reflects predominantly spruce forest with understory herbs such as Chenopodiaceae and *Artemisia*. The pollen assemblage of Layer 2 suggests that the studied area was mainly covered by mixed forests with coniferous and broadleaved trees, consisting mainly of *Larix*, *Betula* and *Corylus*. The understory vegetation is composed of shrub and grassland dominated by Chenopodiaceae, Poaceae and *Artemisia*. The top soil layer (Layer 1) is characterized by the highest pollen and charcoal concentrations compared with other three layers. The pollen assemblage indicates that the area was primarily covered by a mixed coniferous and broadleaf forests dominated by Betula. The other trees include *Corylus*, *Larix*. The understory vegetation consists of herbs such as *Artemisia*, Chenopodiaceae, Poaceae and Leguminosae. The pollen assemblage of this layer was influenced by modern human activities such as ploughing.

4.4. Luminescence and radiocarbon ages

Luminescence properties were first tested to assess the suitability of the SAR method on our samples. A representative OSL decay curve and a dose-response curve for an aliquot of sample

Please cite this article in press as: Zou, G.-N., et al., Geochronology and paleoenvironment of the Taoshan site, northeastern China, and archaeological implications, Quaternary International (2017), http://dx.doi.org/10.1016/j.quaint.2017.06.073

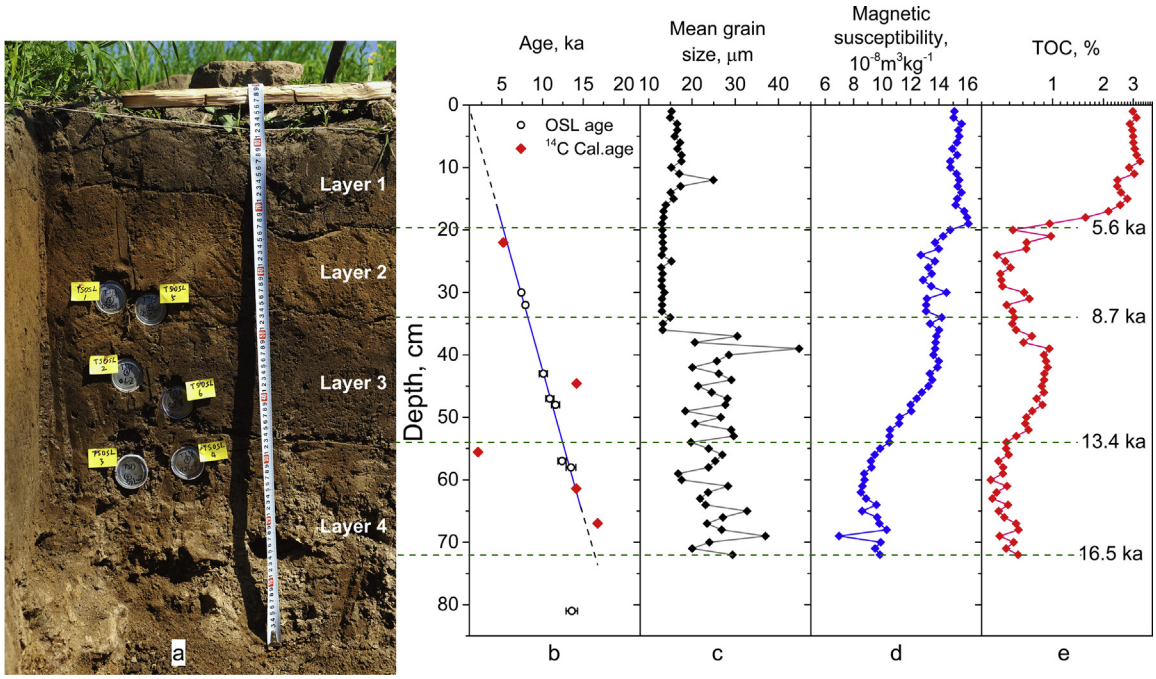

Fig. 3. (a) Photograph of the west section of square F19 showing the stratigraphy and the positions of OSL samples (Samples TS-OSL07 and 08 are not shown); (b) OSL and calibrated radiocarbon ages are plotted against depth, the age points were fitted by a linear function ($R^2 = 0.98$), the boundary ages were obtained by liner interpolation (see text for more details), note that 1σ-error bars are smaller than the size of plot symbols in most cases and the equivalent depths of radiocarbon samples are presented; (c) Mean grain size; (d) magnetic susceptibility and (e) TOC content.

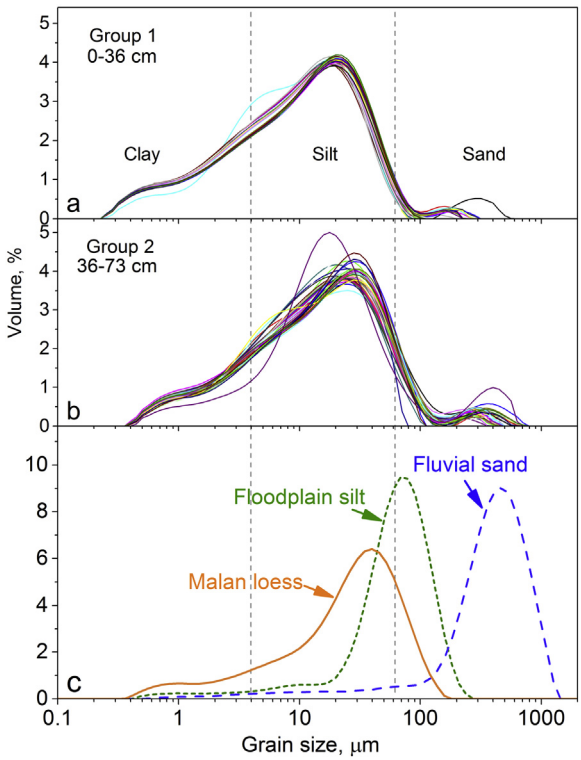

Fig. 4. Grain size distribution curves for the samples from the upper (a) and lower (b) parts of the studied section. The distribution curves for a Malan loess sample from the Chinese Loess Plateau, a typical floodplain silt sample and a fluvial sand sample (Zhang et al., 2010, 2011) are also displayed for comparison (c).

L2503 are shown in Fig. 6a and b. Analyses showed that the OSL signal is rapidly and easily bleached in a few seconds of light exposure, suggesting that the signal is dominated by the fast component. The recycling ratio is within 10% of unity, and the recuperation is much less than 5%. All these observations demonstrate that the SAR method is suitable for our samples. In order to determine preheat temperature for these samples, preheat plateau tests were carried out on sample L2504. The results shown in Fig. 6c demonstrate no dependency of the D_e values on preheat temperature in the range of 160–280 °C. Dose recovery tests were also performed on the same sample to confirm the results of the preheat plateau tests. The dose recovery ratios (the ratio of the measured D_e to the given dose) obtained for different preheat temperature are shown in Fig. 6d. It can be seen that the ratios are consistent in the range of 180–250 °C, and the values indicate that the given dose was adequately recovered. Based on the results of the preheat plateau and dose recovery tests, we selected the preheat of 200 °C for 10 s in this study.

The average D_e values and calculated dose rates obtained for each sample are listed in Table 1. Note that the relative standard errors of the D_e estimates for all samples are less than 3.2%, and the total dose rates for the studied samples are consistent within errors, except for sample L2509 at a depth of 81 cm. OSL ages were calculated by dividing the mean D_e values by the total dose rates, and they are listed in Table 1 and also plotted as a function of depth in Fig. 3b and Fig. S2. The three samples from Layer 4 were dated to 13.6, 13.9 and 12.4 ka, the three samples from Layer 3 to 11.6, 10.9 and 10.1 ka, and the two samples from Layer 2 to 7.9 and 7.4 ka, respectively. The OSL ages are in stratigraphic order.

The conventional and calibrated radiocarbon ages of the five charcoal samples were listed in Table 2, and the calibrated ages are also displayed in Fig. 3b based on their equivalent burial depths in

Please cite this article in press as: Zou, G.-N., et al., Geochronology and paleoenvironment of the Taoshan site, northeastern China, and archaeological implications, Quaternary International (2017), http://dx.doi.org/10.1016/j.quaint.2017.06.073

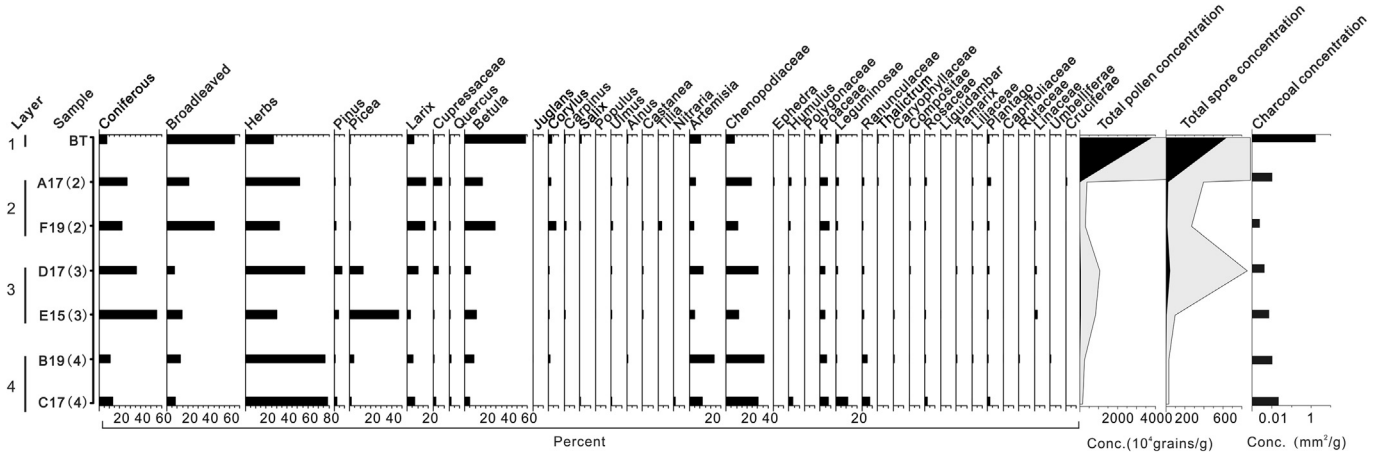

Fig. 5. Percentage pollen diagram, pollen concentration (grains per g bulk sediment) and charcoal content. Note log scale on x-axis for charcoal content.

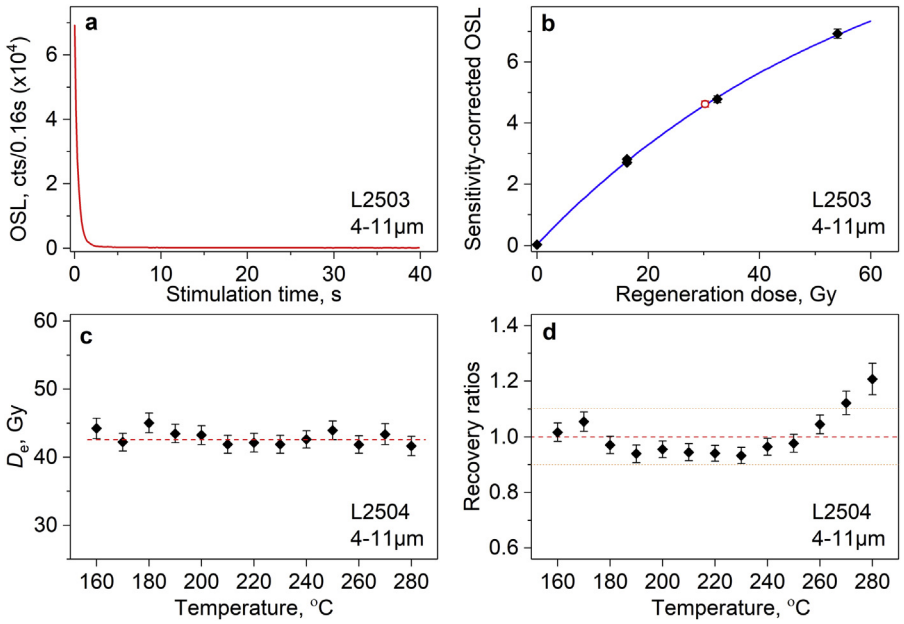

Fig. 6. (a) Decay curve and (b) dose response curve for the fine-grained quartz extracted from sample L2503; (c) De values and (d) dose recovery ratios determined using different preheat temperatures for sample 2504 (see text for further details).

the OSL sampling section. The three charcoal samples (BA141496, BA141495 and BA141493) from Layer 4 are dated to about 16.8, 14.1 and 2.0 cal ka BP. The two charcoal samples (BA141494 and BA131654) from Layers 3 and 2 were dated to 14.2 and 5.2 cal ka BP, respectively.

5. Discussion

5.1. Site chronology and stratigraphic integrity

A total of eight OSL and five radiocarbon dates were determined for the site (Fig. 3b and Fig. S2). As mentioned above, the luminescence properties of the studied sediment samples suggest that they are very suitable for the application of quartz OSL dating; given their aeolian origin, grains in these samples were well bleached prior to burial. This is supported by the stratigraphically more consistent OSL ages. Similar results were also obtained for the Qujialing and Longwangchan archaeological sites in China (Fu et al., 2010; Zhang et al., 2011). We thus conclude that the OSL ages obtained for the samples except for sample L2509 should be reliable. Sample L2509 from the depth of 81 cm has a higher dose rate than other seven samples (Table 1), which may be related to the materials from the granite bedrock. On the other hand, its gamma dose rate calculated from the element contents may be incorrect as the sample was collected too close to the granite bedrock. This is because the penetration range of gamma radiation is over 30 cm in sediments (Aitken, 1998). We thus deduced that the OSL age of sample L2509 may be inaccurate. Therefore, this sample is excluded from further consideration in the following discussion.

The calibrated radiocarbon ages of the charcoal samples (BA131654, BA141495 and BA141496) at depths of 22, 61 and 67 cm are stratigraphically consistent with the OSL ages (Fig. 3b and Fig. S2). However, this is not the case for samples BA141494 at a depth of 45 cm and BA141493 at 56 cm. The former age (14,189 ± 80 cal. yr BP) is too old, and the latter (2035 ± 37 cal. yr BP) is too young when compared with the age values of other

Please cite this article in press as: Zou, G.-N., et al., Geochronology and paleoenvironment of the Taoshan site, northeastern China, and archaeological implications, Quaternary International (2017), http://dx.doi.org/10.1016/j.quaint.2017.06.073

Table 1
Results of optical dating.

Lab No.	Field No.	Archae. Layer	Depth, cm	U, ppm	Th, ppm	K, %	Rb, ppm	Water content[a], %	Dose rate, Gy/ka				Number of aliquots measured	D_e, Gy	OSL age, ka
									α	β	γ	cosmic ray	Total		
L2503	TS-OSL01	2	30	2.86 ± 0.11	12.1 ± 0.33	2.31 ± 0.07	117.0 ± 6.4	17.4	0.45 ± 0.16	2.17 ± 0.06	1.22 ± 0.04	0.25	4.10 ± 0.18	5	30.2 ± 0.2	7.4 ± 0.3
L2507	TS-OSL05	2	32	2.70 ± 0.11	12.5 ± 0.34	2.29 ± 0.07	112.0 ± 6.1	17.3	0.45 ± 0.16	2.15 ± 0.06	1.22 ± 0.04	0.25	4.07 ± 0.18	5	32.0 ± 0.3	7.9 ± 0.3
L2504	TS-OSL02	3	43	3.10 ± 0.11	12.6 ± 0.34	2.38 ± 0.07	108.0 ± 6.1	17.2	0.48 ± 0.17	2.26 ± 0.06	1.28 ± 0.04	0.25	4.27 ± 0.19	5	43.0 ± 0.5	10.1 ± 0.5
L2508	TS-OSL06	3	47	2.79 ± 0.11	12.4 ± 0.33	2.32 ± 0.07	127.0 ± 6.6	17.3	0.46 ± 0.16	2.18 ± 0.06	1.23 ± 0.04	0.25	4.11 ± 0.18	5	44.8 ± 0.7	10.9 ± 0.5
L2510	TS-OSL08	3	48	2.79 ± 0.11	12.7 ± 0.34	2.50 ± 0.07	118.0 ± 6.1	16.7	0.46 ± 0.17	2.32 ± 0.06	1.29 ± 0.04	0.25	4.32 ± 0.18	5	49.9 ± 0.4	11.6 ± 0.5
L2505	TS-OSL03	4	58	2.68 ± 0.11	12.3 ± 0.33	2.43 ± 0.07	116.0 ± 6.3	14.6[a]	0.45 ± 0.16	2.24 ± 0.06	1.24 ± 0.04	0.25	4.18 ± 0.18	7	58.0 ± 0.8	13.9 ± 0.6
L2506	TS-OSL04	4	57	2.82 ± 0.11	12.5 ± 0.34	2.50 ± 0.07	115.0 ± 6.2	14.7[a]	0.46 ± 0.17	2.30 ± 0.06	1.27 ± 0.04	0.25	4.28 ± 0.18	7[b]	53.1 ± 1.7	12.4 ± 0.6
L2509	TS-OSL07	4	81	3.45 ± 0.12	14.5 ± 0.38	2.48 ± 0.07	120.0 ± 6.2	14.9[a]	0.55 ± 0.20	2.41 ± 0.06	1.41 ± 0.04	0.16	4.53 ± 0.21	5	61.4 ± 1.3	13.6 ± 0.7

[a] An uncertainty of 10% was assumed for all samples. For samples L2505, 2506 and 2509 from Layer 4, the water content of 17% was used in dose rate calculation (see main text for further details).
[b] An outlier of 43.0 ± 1.4 Gy was omitted.

charcoal and OSL samples. They are out of stratigraphic order. The young age may be attributed to the fact that the sample was altered/contaminated by meteoric water after deposition (Bird et al., 2002), while the old age may be caused by that the dispersed charcoal fragments might be eroded from older sediments, transported to the site and finally redeposited (Lang and Hönscheid, 1999), and/or it was affected by the "old wood" or "inbuilt age" effect (Schiffer, 1986; Gavin, 2001; Kennett et al., 2002). These two ages are thus considered outliers and excluded from further consideration in this study.

As mentioned above, the archaeological/stratigraphic layers are characterized by different artifact assemblages/archaeological features, especially for Layers 2 and 3. It is necessary to determine the age of the boundary between these layers. A linear age–depth model was constructed using OSL and radiocarbon dates with OriginPro 9.1 software (Fig. 3b and Fig. S2). The linear regression is indicated by the coefficient of determination ($R^2 = 0.98$). Linear interpolation was used to calculate an age for the boundary (Fig. 3b and Fig. S2). The uncertainty associated with each interpolated age is estimated as c. 10%. It is shown that the boundary ages for Layers 4 and 3, 3 and 2, 2 and 1, are about 13.4, 8.7 and 5.6 ka, respectively. The sediment age at the depth of 72 cm was extrapolated to 16.5 ka, which is similar to that of the bottom charcoal sample (BA141496). We thus infer that the age of the basal section is about 16.5 ka.

Stratigraphic integrity is essential to archaeological interpretation and understanding the chronological correlation of archaeological remains and dated materials. As mentioned above, the spatial distribution of the remains and the sediment characteristics indicates that the cultural layers are intact. However, the depositional chronologies of some archaeological sites demonstrate that this is probably not always the case (e.g., Khaweerat et al., 2010; Zhang et al., 2011). The stratigraphic integrity of archaeological deposits is often assessed using luminescence techniques (Bird et al., 2002; Jacobs et al., 2006; David et al., 2007; Feathers et al., 2010). As shown in Fig. 3b, the OSL ages are stratigraphically consistent, and increase linearly with burial depth even within one layer. The internal and stratigraphic consistency of our OSL age estimates implies that the sediments of the site have not been significantly reworked.

5.2. Environmental history of the site

Fig. 4 shows that the shapes of the distribution curves of the studied deposits are similar to those for typical loess samples from the Chinese Loess Plateau (Sun et al., 2004; Yang and Ding, 2004; Zhang et al., 2010; Vandenberghe, 2013), and are different from floodplain silt or fluvial sand samples. This supports the interpretations that the deposits in the archaeological site are primarily of aeolian origin, and the relatively high TOC and pollen contents within Layer 3 (Figs. 3e and 5) support the interpretation of buried soil. This implies that the paleoclimatic proxies used for loess-paleosol deposits can be employed to reconstruct the environment history of the site. The proxies include grain size, magnetic susceptibility, total organic carbon and pollen. For Chinese loess, grain sizes are generally considered to indicate the energy of winter monsoon wind carrying dust from source areas. Larger grains reflect stronger cold-dry winter monsoon, and then indicate more arid climate condition, and the grain size of loess deposits are generally larger than that of paleosols (Liu, 1985; An et al., 1991a; Ding et al., 1992; Xiao et al., 1995; Sun et al., 1999). However, this is not the case for the studied section (Fig. 3c), where the mean grain-size values and the grain-size distribution of the buried soil layer (Layer 3) and loess deposits (Layer 4) are

Please cite this article in press as: Zou, G.-N., et al., Geochronology and paleoenvironment of the Taoshan site, northeastern China, and archaeological implications, Quaternary International (2017), http://dx.doi.org/10.1016/j.quaint.2017.06.073

Table 2
Radiocarbon ages.

Lab No.	Field No.	Archae. layer	Depth, cm[b]	Material	Method	^{14}C age yr BP	Cal. yr BP (1σ)[a]	Cal. age range, yr BP (2σ)[a]
BA131654	07/08C18:T-9-1	2	22	Charcoal	AMS	4535 ± 35	5176 ± 82	5313–5051
BA141494	6117(3)F15:914-1	3	45	Charcoal	AMS	12,275 ± 30	14,189 ± 80	14,360–14044
BA141493	6118(3)C15:1046	4	56	Charcoal	AMS	2065 ± 20	2035 ± 37	2115–1952
BA141495	6128(4)D18:1933	4	61	Charcoal	AMS	12,245 ± 35	14,148 ± 71	14,292–14014
BA141496	6128(4)A18:1985	4	67	Charcoal	AMS	13,860 ± 40	16,781 ± 116	16,999–16557

[a] Calibrated using the online OxCal V4.2 software (Bronk Ramsey, 2009) and the IntCal13 calibration curve (Reimer et al., 2013).
[b] In order to compare with OSL ages, the burial depths of radiocarbon samples are transformed to equivalent depths in the OSL sampling section (see text).

identical. This may be attributed to the source of the loess deposits in Northeast China (Zhu et al., 2013). This is because the grain-size distribution of loess deposits depends, to a large extent, on distance to the dust source and source area environmental conditions, resulting in different interpretations of the grain-size proxy of loess responsible for an additional challenge (see reviews by Vandenberghe, 2013; Újvári et al., 2016). The grain-size proxy is thus not used for further paleoclimatic interpretation in this study.

Magnetic susceptibility of sediments is an indicator reflecting the concentrations of magnetic minerals in the sediments, and widely used as a proxy for paleoprecipitation for Chinese loess (Maher et al., 1994; Maher and Thompson, 1992, 1995), and MS in paleosols is generally higher than in loess (e.g. Kukla et al., 1988; An et al., 1991b). TOC content is closely associated with the vegetation density, and variation in intensity of pedogenesis at the time of dust deposition. High TOC content in soil reflect moist conditions and active pedogenic processes during soil formation, while lower TOC content in loess indicate drier conditions and weaker organic activities (Huang et al., 2003; Basarin et al., 2011). The fossil pollen assemblages have been widely used to reconstruct vegetation history and climate conditions (Li et al., 2011; Liu et al., 2016). Based on the MS, TOC and pollen proxies, the paleoenvironment of the site for the cultural layers is reconstructed.

5.2.1. Layer 4 (16.5–13.4 ka)

This loess layer is characterized by low MS and TOC values (Fig. 3d and e), and a pollen assemblage dominated by Chenopodiaceae and *Artemisia*, indicating less dense woody vegetation cover. These paleoclimate proxies indicate cold and dry climate during this period. Despite a cold and dry climate, stone artifacts indicate human activity during this period.

5.2.2. Layer 3 (13.4–8.7 ka)

The layer consists of Holocene soils. It has higher TOC and pollen

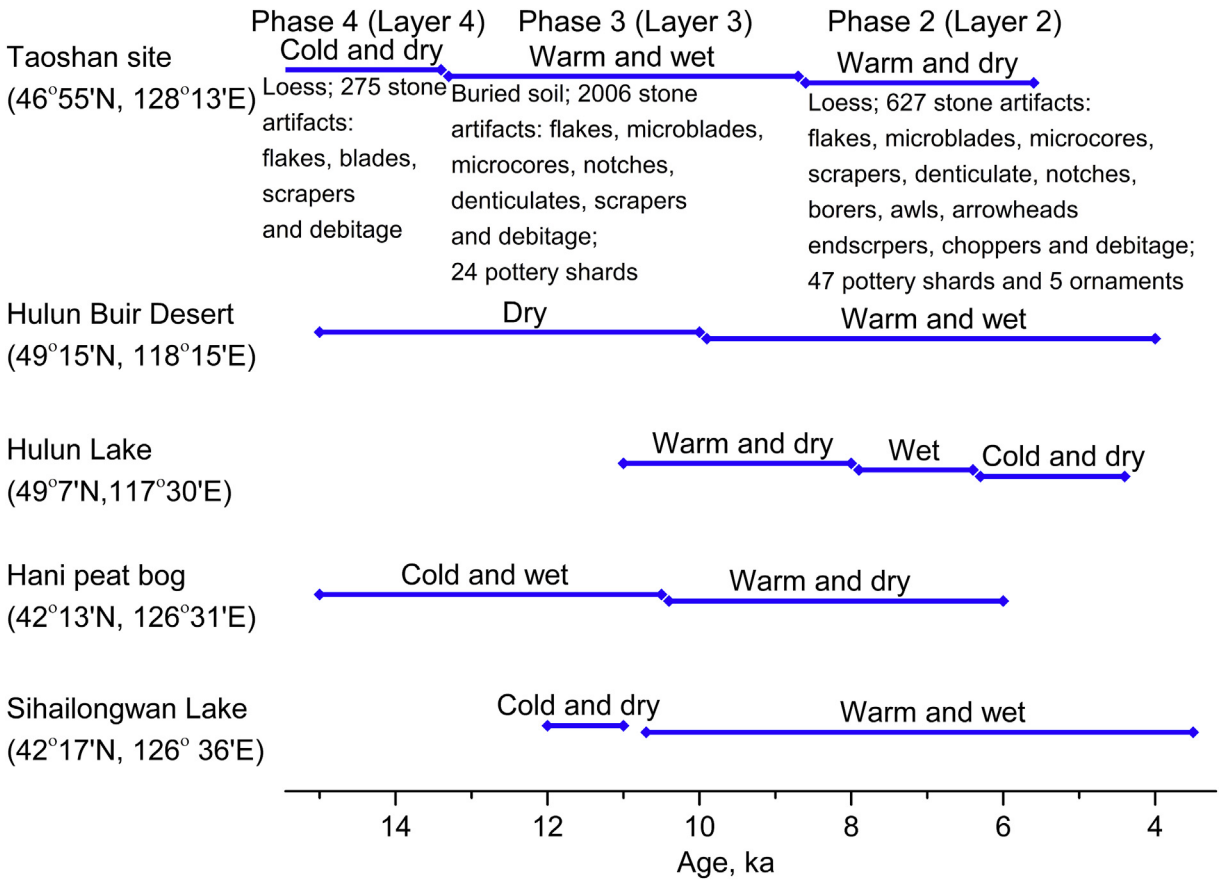

Fig. 7. Comparison of the Holocene climate histories of the study region and other localities in northeastern China. Hulun Buir Desert (Li et al., 2002; Li and Sun, 2006); Hulun Lake (Wen et al., 2010); Hani peat bog (Seki et al., 2009; Zhou et al., 2010); Sihailongwan Lake (Stebich et al., 2015).

Please cite this article in press as: Zou, G.-N., et al., Geochronology and paleoenvironment of the Taoshan site, northeastern China, and archaeological implications, Quaternary International (2017), http://dx.doi.org/10.1016/j.quaint.2017.06.073

content than the overlying and underlying loess layers. The MS values increase from the bottom to the top of the layer. These paleoclimatic proxies suggest strong pedogenesis, and imply warmer and wetter climate during this period, possibly corresponding to the so-called Holocene Optimum (the warmest and wettest period) in China (Shi et al., 1993; An et al., 2000). The optimum climate resulted in the widespread spruce forest in the vicinity of the site. 2006 stone artifacts and 24 pottery sherds from this imply increased human activity at the site during this phase. This might be associated with a warm and wet climate.

5.2.3. Layer 2 (8.7–5.6 ka)

This loess layer has a relatively low TOC content similar to Layer 4, and its MS values slightly decreases from the top of the underlying soil layer (Layer 3). This was also implied an increase in more drought-tolerant species such as *Larix* and Birch. These indicates that the local climate during this phase was warm, and became relatively drier than the earlier stage. During this stage, human activities became more intensified, as demonstrated by more types of stone artifacts, more pottery fragments and the preservation of five ornaments in this layer.

The Holocene climate of northeastern China was previously investigated using multiple proxies, some typical results from different localities (Fig. 1a) are shown in Fig. 7. It is shown that the Holocene climate history obtained for our studied site are not completely consistent with those for other localities in northeastern China. This may be because the Holocene climate evolution in northeastern China was a more regional phenomenon, and the Holocene East Asia summer monsoon precipitation variably affects in different regions at different times (Liu et al., 2015).

5.3. The archaeological and historic significance of the Taoshan site

Archaeologists interpret the presence of many potsherds at this site as a Neolithic feature. However, recent discoveries in other regions of China, as well in Japan, Korea and the Russian far-East, suggest that in East Asia ceramic predate the transition to agriculture in this region by as much as ten thousand years (Cohen, 2013; Shelach, 2012). Thus, technological changes observed during the life-span of this site should not be viewed as a categorical evidence for the beginning of the 'Neolithic' period but rather as part of a long-duration process of 'Neolithization', the process of change from small bands of mobile hunter-gatherer to larger group of sedentary agriculturalists. In north China, this process seems to have taken a long time starting at the height of the last glacial maximum (LGM) age, some 20,000 years ago and reaching full development during the Holocene some 8000 years ago.

It seems that during the LGM this region, and even regions to its south, were abandoned (Qu et al., 2013). With the onset of warmer and wetter conditions during the very late Pleistocene and early Holocene, better environmental conditions coupled with changes in the migration patterns of large game animals and the rise of sea levels, resulted in human migration from the south and east to inland regions and high northern latitudes (Jia, 2007). Phases (Layers) 4, and especially 3 of the Taoshan site seem to reflect the more extensive presence, in the northernmost parts of Northeast China, of groups of mobile hunter-gatherers. The lithic assemblage in this phase is mostly made up of microblades (Chang et al., 2016; Yue et al., 2017) and is similar to that found during this period over a very large region that covers most of North China as well as areas to its north in the Amur region and beyond (Bettinger et al., 2007; Chen, 2007; Shelach, 2015). The production of microblade artifacts represents the spread of advanced technology of lithic production, that arguably spread to this region with the colonizing populations. It is also associated with changing of economic adaptation including, perhaps, the diversification of food resources, including the hunting of smaller animal, intensive gathering of plant resources, as well as the processing of non-food resources such as hide (Elston et al., 2011; Jia, 2007; Shelach, 2015). More research focusing on the procurement of food remains from relevant strata and artifacts should be done to further evaluate the exact nature of the local economy and human diet.

Phase (Layer) 2 of the Taoshan site, which includes evidence for more intensive, though probably not sedentary, occupation as well as evidence for the production and use of ceramic vessels, seem to represent a new phase in the history of this region. Associating the initiation of ceramic production with the beginning of agriculture has a long tradition in Western scholarship and, in spite of growing evidence that hunter-gatherers produced pottery in East Asia and elsewhere (Zvelebil and Jordan, 2009), it is still commonplace for scholars in China and others to make this association, and to equate pottery with the beginning of the Neolithic which is associated with agriculture and sedentary way of life. We take a different approach, inspired by the notion of Neolithization developed in the context of European prehistory. Here we take 'Neolithization' to describes the transition to agriculture and sedentary way of life not as a one-time event but as a long-term process which involves slow-rate technological and social change, the transfer of technologies, including domesticated plans and animals, and the co-existing of communities which rely to various degrees on domesticated and wild resources. Such process eventually resulted in the appearance of fully developed agriculture and of sedentary larger societies, but during the process itself, which took thousands of years, the rate of change was slow and its affects were not necessary evident to the participant societies. In this respect it seems that low-level production of pottery among hunter and gatherer societies, such as that of phase 2 at Taoshan, serve to better utilize existing resources, for example the long cooking of animal bones to extract fat or of hard to digest plants such as seeds. Such technology may have been part of the Neolithization process because it helps reducing the mobility of foragers groups and/or because it enabled the utilization of new resources which later become domesticated (Shelach, 2015). It is interesting that in Taoshan such processes are associated with a period of decreased precipitation and colder average temperatures, suggesting perhaps that new technologies, including ceramic production but also perhaps social mechanisms, were adopted to cope with the stress caused by such conditions. For example, decrease in the animal population that were available for hunting may have forced the Taoshan community to maximize the calorie intake from every animal they succeed hunting through the extensive boiling of the animal bones, as well as to start using plants such as seeds or acorns that needed a long boiling before human can consume them. While we have no direct evidence for the processing of such foods early ceramic is associated with them in other parts of north China (e.g. Liu et al., 2010; Yang et al., 2014).

6. Conclusions

The archaeological deposits of the Taoshan site are made up primarily of grains of aeolian origin, and divided into four layers. Layers 4 and 2 consist of loess deposits characterized by low TOC, and Layers 3 and 1 are composed of soils characterized by relatively high TOC and pollen contents. The quartz OSL dates show excellent stratigraphic coherence, while the charcoal radiocarbon dates show some scatter. OSL demonstrated great utility in dating such archaeological deposits. Excavations recovered a total of 2908 stone artifacts, 74 pottery sherds and five ornaments from Layers 4, 3 and 2. The ages of these three cultural layers (archaeological phases) were determined to be 16.5–13.4 ka for Layer 4, 13.4–8.7 ka for Layer 3 and 8.7–5.6 ka for Layer 2 by linear interpolation and

Please cite this article in press as: Zou, G.-N., et al., Geochronology and paleoenvironment of the Taoshan site, northeastern China, and archaeological implications, Quaternary International (2017), http://dx.doi.org/10.1016/j.quaint.2017.06.073

extrapolation. The multiple paleoclimate proxies indicate that the local climate was cold and dry for the period of 16.5–13.4 ka of Layer 4, in which 275 stone artifacts were found. It was warm and wet for the period of 13.4–8.7 ka of Layer 3, in which 2006 stone artifacts and 24 pottery sherds were excavated. It was warm and dry for the period of 8.7–5.6 ka of Layer 2, in which 627 stone artifacts, 47 pottery sherds and five ornaments were discovered. The paleoclimate change during the human occupation is coupled with the changes in the types and amounts of the archaeological remains including stone artifacts, pottery and ornaments within the cultural layers. This implies that the human-related processes identified at Taoshan are associated with climatic and environmental changes. Especially, the production of pottery, which starts during a period of improved climatic conditions, suggest that such conditions allow for the introduction of new technologies into this region, either by interaction with areas to the south where pottery production already existed or by people who migrated to this region. Under favorable conditions, pottery may have been part of the diversification of human economy, including perhaps the cultivation of plants, however, more research is needed to address these ideas.

Acknowledgments

Funding for this study was provided by undergraduate student research training program of the Ministry of Education for Zou. This study was also supported by the National Natural Science Foundation of China (Grant Nos. 41171007 and 41272033), and the Special Funds of Project for Paleontological Fossils Excavation, Chinese Academy of Sciences (2013 and 2014). Meanwhile, the excavation work at Taoshan site was sponsored by Ya-Mei HOU and her team member Shixia Yang, Yang Chang, Jianping Yue and Yue Hu from Institute of Paleontology and Paleoanthropology, Chinese Academy of Sciences and other co-members like Wei Zhang and Youqian Li from Heilongjiang Provincial Institute of Cultural Relics and Archaeology, Huaidong Hao from Yichun Administrative Station of Cultural Relics, Xuedong Wang from Taoshan Museum and Limin Qiu from Tieli Cultural Relics Station. We thank and appreciate the four anonymous reviewers and the guest editor for their constructive comments on the earlier version of this paper, their valuable comments and suggestions significantly improved the quality of the manuscript.

Appendix A. Supplementary data

Supplementary data related to this article can be found at http://dx.doi.org/10.1016/j.quaint.2017.06.073.

References

Aitken, M.J., 1998. An Introduction to Optical Dating: the Dating of Quaternary Sediments by the Use of Photon-stimulated Luminescence. Oxford University Press, Oxford.
An, Z.S., Kukla, G., Porter, S.C., Xiao, J.L., 1991a. Late quaternary dust flow on the Chinese loess plateau. Catena 18, 125–132.
An, Z.S., Kukla, G., Porter, S.C., Xiao, J.L., 1991b. Magnetic susceptibility evidence of monsoon variation on the Loess Plateau of Central China during the last 130,000 years. Quat. Res. 36, 29–36.
An, Z.S., Porter, S.C., Kutzbach, J.E., Wu, X.H., Wang, S.M., Liu, X.D., Li, X.Q., Zhou, W.J., 2000. Asynchronous Holocene optimum of the east Asian monsoon. Quat. Sci. Rev. 19, 743–762.
Baoding, Diqu Wenwu Guanlisuo, 1991. Hubei Xushui xian Nanzhuangtou yizhi shijue jianbao [preliminary report of the Trail excavation at the Nanzhuangtou site, Xushui county, Hubei]. Kaogu 11, 961–970 (in Chinese).
Basarin, B., Vandenberghe, D.A.G., Marković, S.B., Catto, N., Hambach, U., Vasiliniucb, S., Derese, C., Rončević, S., Vasiljević, Dj.A., Rajićf, Lj, 2011. The Belotinac section (Southern Serbia) at the southern limit of the European loess belt: initial results. Quat. Int. 240, 128–138.
Beijing Daxue Kaogu Wenbo Xueyuan, 2006. Beijingshi Mentougou qu Donghulin shiqian yizhi. Kaogu 7, 3–8 (in Chinese).
Berglund, B.E., 2003. Human impact and climate changes - synchronous events and a causal link? Quat. Int. 105, 7–12.
Bettinger, R., Barton, L., Richerson, P.J., Boyd, R., Wang, H., Choi, W., 2007. The transition to agriculture in northwestern China. In: Madsen, D.B., Chen, F.H., Gao, X. (Eds.), Late Quaternary Climate Change and Human Adaptation in Arid China. Elsevier, Amsterdam, pp. 83–101.
Bird, M.I., Turney, C.S.M., Fifield, L.K., Jones, R., Ayliffe, L.K., Palmer, A., Cresswell, R., Robertson, S., 2002. Radiocarbon analysis of the early archaeological site of Nauwalabila I, Arnhem Land, Australia: implications for sample suitability and stratigraphic integrity. Quat. Sci. Rev. 21, 1061–1075.
Borrero, L.A., Zarate, M., Miotti, L., Massone, M., 1998. The Pleistocene-Holocene transition and human occupations in the southern cone of south America. Quat. Int. 50, 191–199.
Bøtter-Jensen, L., Mejdahl, V., Murray, A.S., 1999. New light on OSL. Quat. Sci. Rev. 18, 303–310.
Bronk Ramsey, C., 2009. Bayesian analysis of radiocarbon dates. Radiocarbon 51, 337–360.
Chang, Y., Hou, Y.-M., Yang, S.-X., Zhang, W., Li, Y.Q., Hao, H.-D., Wang, X.-D., Qiu, L.-M., Yue, J.-P., Hu, Y., 2016. A preliminary report on 2013 excavation of the Taoshan site, Yichun of Heilongjiang Province. Acta Anthropol. Sin. 35, 223–237 (in Chinese with English abstract).
Chen, C., 2007. Techno-typological comparison of microblade cores from east Asia and north America. In: Kuzmin, V.Y., Keates, S.G., Shen, Chen (Eds.), Origin and Spread of Microblade Technology in Northern Asia and North America. Burnaby. Archaeology Press, pp. 7–38.
Clark, J.S., 1988. Particle motion and the theory of charcoal analysis: source area, transport, deposition and sampling. Quat. Res. 30, 67–80.
Cohen, D.J., 2013. The advent and spread of early pottery in East Asia: new considerations and new dates for the world's earliest ceramic vessels. J. Austronesian Stud. 4, 55–92.
David, B., Roberts, R.G., Magee, J., Mialanes, J., Turney, C., Bird, M., White, C., Fifield, L.K., Tibby, J., 2007. Sediment mixing at Nonda Rock: investigations of stratigraphic integrity at an early archaeological site in northern Australia and implications for the human colonization of the continent. J. Quat. Sci. 22, 449–479.
Ding, Z.L., Rutter, N., Han, J.T., Liu, T.S., 1992. A coupled environmental system formed at about 2.5 Ma in East Asia. Palaeogeogr. Palaeoclimatol. Palaeoecol. 94, 223–242.
Elston, R.G., Dong, G., Zhang, D., 2011. Late Pleistocene intensification technologies in northern China. Quat. Int. 242, 401–415.
Faegri, K., Iversen, J., 1989. Textbook of Pollen Analysis (3rd). Blackwell, Oxford, p. 295.
Feathers, J., Kipnis, R., Pilo, L., Arroyo-Kalin, M., Coblentz, D., 2010. How old is Luzia? Luminescence dating and stratigraphic integrity at Lapa Vermelha, Lagoa Santa, Brazil. Geoarchaeology 25, 395–436.
Fu, X., Zhang, J.F., Mo, D.W., Shi, C.X., Liu, H., Li, Y.Y., Zhou, L.P., 2010. Luminescence dating of baked earth and sediments from the Qujialing archaeological site, China. Quat. Geochronol. 5, 353–359.
Gavin, D.G., 2001. Estimation of inbuilt age in radiocarbon ages of soil charcoal for fire history studies. Radiocarbon 43, 27–44.
Guo, R.H., Li, J., 2002. The Nanzhuangtou and Hutouliang sites: exploring the beginnings of agriculture and pottery in North China. In: Yasuda, Y. (Ed.), The Origins of Pottery and Agriculture. Roli Books, New Delhi, pp. 193–204.
Guo, Y.Y., Mo, D.W., Mao, L.J., Jin, Y.X., Guo, W.M., Mudie, P.J., 2014. Settlement distribution and its relationship with environmental changes from the Paleolithic to Shang-Zhou period in Liyang Plain, China. Quat. Int. 321, 29–36.
Grimm, E.C., 1990. TILIA and TILIA.GRAPH. PC spreadsheet and graphics software for pollen data. INQUA, Working Group in Data-handling Methods. Newsletter 4, 5–7.
Hebei Sheng Wenwu Yanjiusuo, et al., 2010. 1997 nian Hebei Xushui Nanzhuangtou yizhi fajue baogao [report on the 1997 excavations at the Nanzhuangtou site, Xushui county, Hebei province]. Kaogu Xuabao 3, 361–392.
Huang, C.C., Pang, J.L., Chen, S.E., Zhang, Z.P., 2003. Holocene dust accumulation and the formation of polycyclic cinnamon soils (luvisols) in the Chinese Loess Plateau. Earth Surf. Process. Land. 28, 1259–1270.
Jacobs, Z., Duller, G.A.T., Wintle, A.G., Henshilwood, C.S., 2006. Extending the chronology of deposits at Blombos Cave, South Africa, back to 140 ka using optical dating of single and multiple grains of quartz. J. Hum. Evol. 51, 255–273.
Jia, W.-M., 2007. Transition from Foraging to Farming in Northeast China. BAR International Series, Oxford, pp. 62–63.
Kato, S., 2016. The use of lithic raw materials during the Upper Paleolithic in eastern China: a focus on microblade industries. Quat. Int. http://dx.doi.org/10.1016/j.quaint.2016.05.006.
Kennett, D.J., Ingram, B.L., Southon, J.R., Wise, K., 2002. Differences in 14C age between stratigraphically associated charcoal and marine shell from the archaic period sites of kilometer 4, southern Peru: old wood or old water? Radiocarbon 44, 53–58.
Khaweerat, S., Weisler, M., Zhao, J.X., Feng, Y.X., Yu, K.F., 2010. Human-caused stratigraphic mixing of a coastal Hawaiian Midden during prehistory: implications for interpreting cultural deposits. Geoarchaeology 25, 527–540.
Kukla, G.J., Heller, F., Liu, S.M., Xu, T.C., Liu, T.S., An, Z.S., 1988. Pleistocene climates dated by magnetic susceptibility. Geology 16, 811–814.
Kuzmin, V.Y., 2006. Chronology of the earliest pottery in East Asia: progress and pitfalls. Antiquity 80, 362–371.
Lang, A., Hönscheid, S., 1999. Age and source of colluvial sediments at Vaihingen-Enz, Germany. Catena 38, 89–107.

Li, S.H., Sun, J.M., Zhao, H., 2002. Optical dating of dune sands in the northeastern deserts of China. Palaeogeogr. Palaeoclimatol. Palaeoecol. 181, 419–429.
Li, S.H., Sun, J.M., 2006. Optical dating of Holocene dune sands from the Hulun Buir Desert, northeastern China. Holocene 16, 457–462.
Li, X.Q., Du, N.Q., 1999. The acid-alkali-free analysis of Quaternary pollen. Acta Bot. Sin. 41, 782–784 (in Chinese with English abstract).
Li, X.Q., Zhao, K.L., Dodson, J., Zhou, X.Y., 2011. Moisture dynamics in central Asia for the last 15 kyr: new evidence from Yili Valley, Xinjiang, NW China. Quat. Sci. Rev. 30, 3457–3466.
Liu, C.L., Zhang, J.-F., Jiao, P.C., Mischke, S., 2016. The Holocene history of Lop Nur and its palaeoclimate implications. Quat. Sci. Rev. 148, 163–175.
Liu, J.B., Chen, J.H., Zhang, X.J., Li, Y., Rao, Z.R., Chen, F.H., 2015. Holocene East Asian summer monsoon records in northern China and their inconsistency with Chinese stalagmite δ^{18}o records. Earth Sci. Rev. 148, 194–208.
Liu, K.X., Ding, X.F., Fu, D.P., Pan, Y., Wu, X.H., Guo, Z.Y., Zhou, L.P., 2007. A new compact AMS system at Peking University. In: Nuclear Instruments and Methods in Physics Research Section B: Beam Interactions with Materials and Atoms, vol. 259, pp. 23–26.
Liu, L., Field, J., Fullagar, R., Bestel, S., Ma, X., Chen, X., 2010. What did grinding stones grind? new light on early Neolithic subsistence economy in the middle Yellow River valley, China. Antiquity 84, 816–833.
Liu, T.S., 1985. Loess and the Environment. China Ocean Press, Beijing.
Maher, B.A., Thompson, R., 1992. Paleoclimatic significance of the mineral magnetic record of the Chinese loess and paleosols. Quat. Res. 37, 155–170.
Maher, B.A., Thompson, R., 1995. Palaeorainfall reconstructions from pedogenic magnetic susceptibility variations in the Chinese loess and palaeosols. Quat. Res. 44, 383–391.
Maher, B.A., Thompson, R., Zhou, L.P., 1994. Spatial and temporal reconstructions of changes in the Asian palaeomonsoon: a new mineral magnetic approach. Earth Planet. Sci. Lett. 125, 461–471.
Murray, A.S., Wintle, A.G., 2000. Luminescence dating of quartz using an improved single-aliquot regenerative-dose protocol. Radiat. Meas. 32, 57–73.
Naudinot, N., Kelly, R.L., 2017. Climate change and archaeology. Quat. Int. 128, 1–2.
Peck, R.M., 1974. A comparison of four absolute pollen preparation techniques. New Phytol. 73, 567–587.
Qu, T., Bar-Yosef, O., Wang, Y., 2013. The Chinese upper paleolithic: geography, chronology, and Techno-typology. J. Archaeol. Res. 21, 1–73.
Reimer, P.J., Bard, E., Bayliss, A., Beck, J.W., Blackwell, P.G., Bronk Ramsey, C., Buck, C.E., Cheng, H., Edwards, R.L., Friedrich, M., Grootes, P.M., Guilderson, T.P., Haflidason, H., Hajdas, I., Hatté, C., Heaton, T.J., Hoffmann, D.L., Hogg, A.G., Hughen, K.A., Kaiser, K.F., Kromer, B., Manning, S.W., Niu, M., Reimer, R.W., Richards, D.A., Scott, E.M., Southon, J.R., Staff, R.A., Turney, C.S.M., van der Plicht, J., 2013. IntCal13 and Marine13 radiocarbon age calibration curves 0-50,000 years cal BP. Radiocarbon 55, 1869–1887.
Schiffer, M.B., 1986. Radiocarbon dating and the "old wood" problem: the case of the Hohokam chronology. J. Archaeol. Sci. 13, 13–30.
Seki, O., Meyers, P.A., Kawamura, K., Zheng, Y., Zhou, W., 2009. Hydrogen isotopic ratios of plant wax *n*-alkanes in a peat bog deposited in northeast China during the last 16 kyr. Org. Geochem. 40, 671–677.
Shelach, G., 2012. On the invention of pottery. Science 336, 1644–1645.
Shelach, G., 2015. The Archaeology of Ancient China: from Prehistory to the Han Dynasty. Cambridge University Press, Cambridge, pp. 50–60.
Shi, Y., Kong, Z., Tang, L., Wang, F., Yao, T., Zhao, X., Zhang, P., Shi, S., 1993. Mid-Holocene climates and environments in China. Glob. Planet. Change 7, 219–233.
Stebich, M., Rehfeld, K., Schlutz, F., Tarasov, P.E., Liu, J.Q., Mingram, J., 2015. Holocene vegetation and climate dynamics of NE China based on the pollen record from Sihailongwan Maar Lake. Quat. Sci. Rev. 124, 275–289.
Sun, D.H., Bloemendal, J., Rea, D.K., An, Z.S., Vandenberghe, J., Lu, H.Y., Su, R.X., Liu, T.S., 2004. Bimodal grain-size distribution of Chinese loess, and its palaeoclimatic implications. Catena 55, 325–340.
Sun, J.M., Ding, Z.L., Liu, T.S., Rokosh, D., Rutter, N., 1999. 580,000-year environmental reconstruction from aeolian deposits at the Mu Us Desert margin, China. Quat. Sci. Rev. 18, 1351–1364.
Tsakalos, E., Christodoulakis, J., Charalambous, L., 2015. The dose rate calculator (DRc) for luminescence and ESR dating—a Java application for dose rate and age determination. Archaeometry 53, 814–819.
Újvári, G., Kok, J.F., Varga, G., Kovács, J., 2016. The physics of wind-blown loess: implications for grain size proxy interpretations in Quaternary paleoclimate studies. Earth Sci. Rev. 154, 247–278.
Vandenberghe, J., 2013. Grain size of fine-grained windblown sediment: a powerful proxy for process identification. Earth Sci. Rev. 121, 18–30.
Wang, Jian, et al., 1978. Xiachuan Wenhua: Shanxi Xiachuan yizhi diaocha baogao [the Xiachuan culture: report on investigations of the Xiachuan site in Shanxi province]. Kaogu Xuabao 3, 259–288.
Wen, R.L., Xiao, J.L., Chang, Z.G., Zhai, D.Y., Xu, Q.H., Li, Y.C., Itoh, S., Lomtatidze, Z., 2010. Holocene climate changes in the mid-high-latitude-monsoon margin reflected by the pollen record from Hulun Lake, northeastern Inner Mongolia. Quat. Res. 73, 293–303.
Wintle, A.G., Murray, A.S., 2006. A review of quartz optically stimulated luminescence characteristics and their relevance in single-aliquot regeneration dating protocols. Radiat. Meas. 41, 369–391.
Wu, X., Zhang, C., Goldberg, P., Cohen, D., Pan, Y., Arpin, T., Bar-Yosef, O., 2012. Early pottery at 20,000 years ago in Xianrendong cave, China. Science 336, 1696–1700.
Xiao, J.L., Porter, S.C., An, Z.S., Kumai, H., Yoshikawa, S., 1995. Grain size of quartz as an indicator of winter monsoon strength on the Loess Plateau of central China during the last 130,000 yr. Quat. Res. 43, 22–29.
Yang, S.L., Ding, Z.L., 2004. Comparison of particle size characteristics of the Tertiary 'red clay' and Pleistocene loess in the Chinese Loess Plateau: implications for origin and sources of the 'red clay'. Sedimentology 51, 77–93.
Yang, S.-X., Zhang, Y.-X., Li, Y.-Q., Zhao, C., Li, X.-Q., Yue, J.-P., Hou, Y.-M., Zhu, R.X., Deng, C.-L., Petraglia, M.D., 2017. Environmental change and raw material selection strategies at Taoshan: a terminal Late Pleistocene to Holocene site in north-eastern China. J. Quat. Sci. http://dx.doi.org/10.1002/jqs.2950.
Yang, X., Ma, Z., Wang, T., Perry, L., Li, Q., Huan, X., Yu, J., 2014. Starch grain evidence reveals early pottery function cooking plant foods in North China. Chin. Sci. Bull. 59, 4352–4358.
Yasuda, Y., Fujiki, T., Nasu, H., Kato, M., Morita, Y., Mori, Y., Kanehara, M., Toyama, S., Yano, A., Okuno, M., He, J.J., Ishihara, S., Kitagawa, H., Fukusawa, H., Naruse, T., 2004. Environmental archaeology at the Chengtoushan site, Hunan Province, China, and implications for the environmental change and the rise and fall of the Yangtze River civilization. Quat. Int. 123, 149–158.
Yue, J.P., Hou, Y.M., Yang, S.X., Chang, Y., Zhang, W., Li, Y.Q., Hao, H.D., Wang, X.D., Qiu, L.M., 2017. A preliminary report on the 2014 excavation at Taoshan site in Heilongjiang province, northeast China. Acta Anthropol. Sin. 36 http://dx.doi.org/10.16359/j.cnki.cn11-1963/q.2017.0013 (in Chinese with English abstract).
Zhang, J.-F., Qiu, W.-L., Wang, X.-Q., Hu, G., Li, R.-Q., Zhou, L.-P., 2010. Optical dating of a hyperconcentrated flow deposit on a Yellow River terrace in Hukou, Shaanxi, China. Quat. Geochronol. 5, 194–199.
Zhang, J.F., Wang, X.Q., Qiu, W.L., Shelach, G., Hu, G., Fu, X., Zhuang, M.G., Zhou, L.P., 2011. The paleolithic site of Longwangchan in the middle Yellow River, China: chronology, paleoenvironment and implications. J. Archaeol. Sci. 38, 1537–1550.
Zhang, J.-F., Zhou, L.-P., 2007. Optimization of the 'double SAR' procedure for polymineral fine grains. Radiat. Meas. 42, 1475–1482.
Zhongguo Shehui Kexueyuan Kaogu Yanjiusuo, Shaanxi Sheng Kaogu Yanjiusuo, 2007. Shaanxi Yichuan xian Longwangchan jiushiqi shidai yizhi [the paleolithic site of Longwangchan, Yichuan county, Shaanxi]. Kaogu 2007 (7), 3–8 (in Chinese).
Zhou, W.J., Zheng, Y.H., Meyers, P.A., Jull, A.J.T., Xie, S.C., 2010. Postglacial climate-change record in biomarker lipid compositions of the Hani peat sequence, Northeastern China. Earth Planet. Sci. Lett. 294, 37–46.
Zhu, J.Y., Mingram, J., Brauer, A., 2013. Early Holocene aeolian dust accumulation in northeast China recorded in varved sediments from Lake Sihailongwan. Quat. Int. 290, 299–312.
Zvelebil, M., Jordan, P., 2009. Ceramics before Farming: the Dispersal of Pottery Among Prehistoric Eurasian Hunter-gatherers. Left Coast Press, Walnut Creek.

Please cite this article in press as: Zou, G.-N., et al., Geochronology and paleoenvironment of the Taoshan site, northeastern China, and archaeological implications, Quaternary International (2017), http://dx.doi.org/10.1016/j.quaint.2017.06.073